A Multiplex Droplet Digital PCR Assay for Chromosome Copy Number Determination in *Candida albicans*

Eli Isael Maciel[1], Sylvain Ursuegui[2], Sana Ahmed-Seghir[2], Corinne Maufrais[1,3,4], Stéphanie Roy[2], Cecile Gautier[1], Philipp Brandt[1,4], Cécile Jovelet[2], Laras Pitayu[2], Iuliana V. Ene[1,*]

[1] Institut Pasteur, Université Paris Cité, Fungal Heterogeneity Group, Paris 75015, France

[2] Life Science Group, Bio-Rad Laboratories, Inc. (LSG PARIS), Villejuif 94280, France

[3] Institut Pasteur Bioinformatic Hub, Université Paris Cité, Paris 75015, France

[4] Institut Pasteur, Université Paris Cité, Fungal Biology and Pathogenicity Unit, Paris 75015, France

* correspondence: iuliana.ene@pasteur.fr

Keywords: aneuploidy; copy number variation; high-order multiplexing; color-combination encoding

Running title: 16-plex ddPCR for *C. albicans* aneuploidy

Abstract

Chromosome copy number variation (CNV) is a major contributor to genome plasticity and adaptation in *Candida albicans*, a leading fungal pathogen of humans. Aneuploidy, defined as deviations from the normal diploid chromosome set, rapidly alters gene dosage, enabling tolerance to host-imposed and antifungal stress. Accurate detection and quantification of chromosomal copy number changes are thus essential to dissect the mechanisms by which *C. albicans* adapts and evolves. Here, we describe the development, optimization, and validation of a six-color, 16-plex droplet digital PCR assay for simultaneous quantification of all *C. albicans* chromosome arms in a single reaction. Each target is detected by a unique dual-color or single-color combination of probes, enabling high-order multiplexing through binary fluorescence encoding. Following optimization of probe concentrations, PCR cycling parameters, genomic DNA extraction and pre-treatment with restriction enzymes, the assay provides accurate, reproducible chromosome-level copy number estimates that correlate closely with WGS results across euploid and aneuploid isolates. Compared to whole-genome sequencing, the assay is rapid, cost-effective, and scalable, requiring minimal DNA input and allowing high-throughput analysis of large isolate collections. The 16-plex assay thus provides a platform for dissecting genome instability and adaptive evolution in *C. albicans*.

Article Summary

We developed and validated a 16-plex droplet digital PCR assay that estimates chromosome dosage across the entire genome of the human fungal pathogen *C. albicans* in a single reaction. The assay uses six fluorescent colors and unique color combinations to track one marker on each chromosome arm, enabling rapid detection of aneuploidy (extra or missing chromosomes). Results closely matched whole-genome sequencing for isolates with simple aneuploid forms and detected low-

frequency trisomic clones in mixed populations. With optimized DNA preparation, this method provides a practical tool for screening genome instability in research and clinical settings.

Introduction

Aneuploidy, the presence of abnormal numbers of chromosomes, is a hallmark of genome instability and a major driver of adaptive evolution across diverse biological systems (Torres et al. 2008; Li and Zhu 2022). In cancer, aneuploidy fuels tumor heterogeneity, promotes rapid adaptation to therapy, and contributes to disease progression (Li and Zhu 2022; Vasudevan et al. 2021). The capacity for karyotypic plasticity is particularly evident in human fungal pathogens, where aneuploidy has emerged as a pervasive mechanism of adaptation to host environments and antifungal stress. Here, it enables rapid adaptation to environmental and drug-induced stress by altering gene dosage without requiring point mutations (Todd and Selmecki 2020; Tsai and Nelliat 2019; Bennett et al. 2014; Vande Zande et al. 2023).

Among fungal pathogens, *C. albicans* exemplifies the dual nature of aneuploidy as both a source of genetic innovation and a contributor to phenotypic variability. *C. albicans* is an opportunistic commensal capable of causing life-threatening systemic infections in immunocompromised individuals (Denning 2024; Brown et al. 2012; Pappas et al. 2018). The remarkable genomic plasticity of this species underlies its ability to thrive in fluctuating host niches and in the presence of antifungal drugs (Selmecki et al. 2010). Unlike most fungi, *C. albicans* lacks a complete sexual cycle, limiting its ability to shuffle alleles through meiosis (Ene and Bennett 2014). Instead, it exploits single point mutations, aneuploidy, loss of heterozygosity, and parasexual recombination to generate genetic diversity (Vande Zande et al. 2023; Todd et al. 2019; Forche 2014; Morrow and Fraser 2013; Selmecki et al. 2010; Bennett et al. 2014).

Aneuploidy has been repeatedly observed in clinical isolates and experimental populations, often associated with adaptation to host niches and antifungal resistance. For example, monosomy of

61 chromosome (Chr) 5 promotes tolerance to fluconazole and caspofungin (Yang et al. 2019), trisomy of
62 Chr2 confers cross-resistance to caspofungin, tunicamycin, and hydroxyurea (Yang et al. 2021a), while
63 duplication of the left arm of Chr5 (iso-Chr5L) drives fluconazole resistance (Selmecki et al. 2008;
64 Selmecki et al. 2006). Despite frequent fitness trade-offs associated with aneuploidy (Zhu et al. 2018;
65 Yang et al. 2021b; Tsai et al. 2019; Tsai and Nelliat 2019; Torres et al. 2007), aneuploid isolates can also
66 facilitate adaptation to mammalian host niches. Acquisition of a Chr7 trisomy enhances colonization of
67 the murine gastrointestinal tract by increasing *NRG1* copy numbers and suppressing filamentation (Ene
68 et al. 2018; Kakade et al. 2023). Trisomy of Chr5 and Chr6 increases fitness for the murine oral cavity,
69 which was associated with decreased epithelial adherence and invasion (Forche et al. 2018). These
70 findings highlight aneuploidy as a powerful, reversible adaptive mechanism that enables *C. albicans* to
71 fine-tune its physiology in response to environmental and host-imposed stresses, balancing the costs
72 of genomic instability with context-dependent fitness gains that enhance survival, persistence, and
73 pathogenic potential.

74 Accurate determination of chromosome copy number and identity is therefore critical for
75 dissecting the role of aneuploidy in fungal adaptation. Whole-genome sequencing (WGS) remains the
76 gold standard for this purpose, providing genome-wide resolution and quantitative accuracy. However,
77 its cost, turnaround time, and computational requirements limit its use in large-scale or high-
78 throughput studies. Alternative methods, such as flow cytometry and quantitative PCR (qPCR), provide
79 faster and more accessible options but suffer from limitations: flow cytometry detects total DNA content
80 without chromosome identity, while qPCR is constrained by limited multiplex capacity and reliance on
81 reference gene normalization.

82 Droplet digital PCR (ddPCR) enables accurate absolute quantification by partitioning a sample
83 into thousands of nanodroplets in which amplification proceeds independently. Applying Poisson
84 statistics to the fraction of positive droplets yields precise copy-number estimates without the need for

85 standard curves. In conventional digital PCR (dPCR), each target is detected with a specific fluorescent
86 probe in a single detection channel, so multiplexing capacity is constrained by the limited number of
87 optical channels. To overcome this, higher-order multiplexing methods use different fluorescence
88 intensities (amplitude- or ratio-based approaches) to encode multiple targets within the same channel.
89 However, these methods require complex multi-level thresholding and are less robust because
90 fluorescence intensity can vary across samples. An alternative approach is color-combination, in which
91 a unique color signature defines each target. While this is impractical in qPCR (because overlapping bulk
92 fluorescence signals create ambiguity), dPCR can precisely identify color combinations in each partition
93 and exclude ambiguous co-encapsulation events. This color-combination approach has been
94 successfully implemented on six-color and seven-color multiplex dPCR platforms, enabling detection of
95 up to 15 and 21 targets, respectively. Importantly, the analysis remains simple and robust: only one
96 threshold per fluorescence channel is required, and dedicated analysis software can automatically
97 identify and quantify targets based on predefined color codes (Santos-Barriopedro 2023). This approach
98 substantially expands multiplexing capacity beyond conventional methods and minimizes competition
99 between primer-probe sets.

100 In this study, we designed, optimized, and validated a 16-plex ddPCR assay for *C. albicans* that
101 measures copy number across all 16 chromosome arms in a single reaction. The panel enables genome-
102 wide quantification with single-reaction throughput and accuracy comparable to WGS. We describe the
103 assay development process, including probe design and refinement of underperforming loci,
104 optimization of DNA extraction and digestion, PCR cycling conditions, and calibration of fluorescence
105 compensation. We then show that the assay detects mixed euploid-aneuploid populations and validate
106 its quantitative precision by comparison with WGS-derived copy number profiles across a diverse strain
107 panel. Together, these results establish the 16-plex ddPCR assay as a rapid, scalable, and quantitative
108 approach for genome-wide aneuploidy detection in *C. albicans*.

109

110 **Methods**

111 ***C. albicans* strains and growth.** All experiments were performed using *C. albicans* isolates representing
112 a range of karyotypes. The reference strain SC5314 (euploid A) served as one of the main euploid
113 controls. For sensitivity testing in mixed populations, disomic and aneuploid subpopulations derived
114 from the same genetic background (euploid B, CAY6440) were combined in defined ratios (25%, 50%,
115 and 75% aneuploid). The collection of isolates used throughout the study is available in **Supplementary**
116 **Table 1.** Yeast cells were cultured in YPD medium (1% yeast extract, 2% peptone, and 2% dextrose)
117 overnight at 30°C with shaking (200 rpm). Cells were collected from the stationary phase for genomic
118 DNA extraction.

119

120 **Genomic DNA extraction.** The yeast strains were grown on agar or liquid YPD medium for DNA
121 extraction. Two extraction methods were evaluated for their effects on assay performance: a phenol–
122 chloroform method and a QIAGEN Genomic-tip column-based kit (10223, QIAGEN).

123 For phenol-chloroform extractions, 2 mL of an overnight culture or a patch of cells from a plate
124 was washed twice with sterile water and resuspended in 400 µL TE (Tris-EDTA, pH 8) buffer containing
125 20 µL 20% SDS and 200 µL phenol:chloroform:isoamyl alcohol (25:24:1, neutral pH). Cells were lysed by
126 bead beating (FastPrep, three cycles of 20 s at power setting 4, with a 3 min rest on ice between cycles).
127 The aqueous phase was recovered, and the DNA was precipitated with ethanol and washed with 70%
128 ethanol. Residual RNA was removed with RNase treatment.

129 Column-based extractions were performed according to the manufacturer's instructions
130 (QIAGEN). Briefly, 2 mL of an overnight culture or a patch of cells from a plate was washed with 1X TE
131 buffer, the cell wall was digested with Lyticase (L2524, Sigma) in buffer Y1 for 1 h, followed by treatment
132 with Proteinase K (P2308, Sigma) and RNase (R5503, Sigma) in buffer G1. The DNA was purified using

133 Genomic-tip columns, eluted, precipitated with isopropanol, washed with 70% cold ethanol, and
134 resuspended in sterile water.
135
136 **DNA digestion.** Restriction enzyme digestion was tested using FastDigest enzymes (Thermo Fisher)
137 BamHI (FD0054), EcoRI (FD0274), HindIII (FD0504), and PstI (FD0614). Each reaction contained 3 µg of
138 genomic DNA, which was digested for 30 min according to the manufacturer's recommended
139 conditions. Digested DNA was quantified and diluted to final template concentrations of 10 or 30 pg per
140 reaction. Single-enzyme and combination digestions were tested systematically. SnapGene Viewer was
141 used to verify enzyme restriction sites.
142
143 **Target Selection and Probe Design.** The *C. albicans* Crystal digital PCR assay (R52002, Stilla
144 Technologies, Bio-Rad Laboratories) was designed to quantify chromosome copy number at 16 loci, one
145 per chromosome arm. Additional assay details, including recommended reaction concentrations,
146 validated restriction enzymes, thermocycling programs, and instructions for image and data analysis,
147 are provided in the assay information sheet (https://go.stillatechnologies.com/assay/c-albicans-
148 crystal-digital-pcr-r-assay).
149 To minimize sequence or copy number variation that might affect probe binding, candidate loci
150 were chosen based on three principles: near diploid coverage in the SC5314 reference strain, proximity
151 to centromeric regions, and the potential for high gene conservation due to essential or housekeeping
152 function. Each target was verified against the SC5314 reference genome (assembly 22) to confirm the
153 absence of restriction enzyme cut sites within the amplicon (**Supplementary Table 2**). The final targets,
154 fluorophore combinations, and encoding schemes are listed in **Supplementary Table 3**. Probes used in
155 this study were designed using Flex Probe and Universal Reporter Technology (Stilla Technologies, Bio-
156 Rad Laboratories). Flex Probes are target-specific, non-fluorescent probe oligonucleotides that trigger

157 the fluorescence of Universal Reporters in the presence of the targeted sequence. To design the
158 oligonucleotides, the SC5314 assembly 22 was used. Sequence homology with species closely related
159 to *C. albicans* (e.g., *Candida dubliniensis*, *Candida tropicalis*) was assessed using BLAST, and the primer
160 and probe design were adjusted accordingly. Each target was first tested individually (simplex) and then
161 as part of the 16-plex mixture. Simplex reactions yielded higher apparent copy numbers (reflecting
162 reduced competition), but multiplex reactions preserved expected chromosome ratios and produced
163 reproducible results after probe re-design and digestion.
164
165 **Reaction mix preparation and PCR cycling conditions.** For each reaction, 0.6 µL Crystal Flex probes
166 and primers were mixed with 0.6 µL 10X Buffer A, 0.24 µL 10X Buffer B, 0.15 µL Universal Reporter A, 0.15
167 µL Universal Reporter B (all naica PCR MIX reagents (R10106) and Universal Reporters 7 (R42401), Stilla
168 Technologies, Bio-Rad Laboratories), and 4.3 µL of 14 or 42 pg/µL genomic DNA (gDNA) template.
169 Primers and Flex Probes are listed in **Supplementary Table 4**. A total of 5 µL of the prepared reaction
170 mixture was loaded into each chamber of a Ruby Chip (C16011, Stilla Technologies, Bio-Rad
171 Laboratories). The chip was loaded into the dPCR cycler (naica Geode, Stilla Technologies, Bio-Rad
172 Laboratories), a device that combines droplet generation and thermocycling. Following droplet
173 partitioning, the amplification protocol was initiated, consisting of an initial denaturation at 95°C for 3
174 min, followed by 60 cycles of 15 s at 95°C for denaturation and 45 s at 60°C for annealing and elongation.
175 A final elongation step at 58°C for 15 min was performed before chip release. Alternate programs tested
176 included extended elongation (60 s) and final elongation durations (10 or 15 min). Longer elongation at
177 60 s and a final elongation of 15 min improved separability scores, simplifying thresholding and
178 improving left/right arm balance, especially for low-amplitude targets (e.g., Chr4R). Increasing probe
179 concentrations from 0.5 µM to 1 µM further improved amplitude and reduced uncertainty.

To quantify the discrimination between positive and negative ddPCR droplets, we used a separability score (S), calculated by Crystal Miner, that incorporates both the magnitude of signal separation and the variability within each droplet population (**Supplementary Figure 1**). For each ddPCR reaction, droplets were partitioned into positive and negative populations based on fluorescence amplitude. The separability score was then calculated as:

$$S = \frac{\mu_{\text{pos}} - \mu_{\text{neg}}}{\sqrt{\frac{p}{p-1}}\,\sigma_{\text{pos}} + \sqrt{\frac{q}{q-1}}\,\sigma_{\text{neg}}}$$

Where $\mu_{\text{pos}}$and $\mu_{\text{neg}}$are the mean fluorescence amplitudes of the positive and negative droplet populations, respectively; $\sigma_{\text{pos}}$and σ_{neg} are the corresponding standard deviations; p and q are the number of positive and negative droplets, respectively. A higher score indicates greater separation between positive and negative droplets, reflecting improved resolution. This metric provides a normalized measure of ddPCR performance that accounts for both signal dispersion and population size.

Fluorescence Detection and Compensation. The chips were scanned using the dPCR reader (naica Prism6, Stilla Technologies, Bio-Rad Laboratories), which is equipped with six fluorescence channels (blue, teal, green, yellow, red, and infrared (IR)). Exposure times were optimized for each channel: Blue = 500 ms, Teal = 800 ms, Green = 250 ms, Yellow = 350 ms, Red = 1000 ms, IR = 1000 ms. To correct for spectral overlap, a spillover compensation matrix (Madic et al. 2016) was generated using mono-color control reactions and implemented in the Crystal Miner v4.0 software (Stilla Technologies, Bio-Rad Laboratories). The validated matrix was applied consistently across all experiments. Thresholds were manually adjusted to lie midway between positive and negative clusters.

202 **Whole-genome sequencing and coverage analysis.** *C. albicans* cells were cultured in 5 mL YPD
203 medium overnight at 30°C with continuous shaking at 200 rpm. The DNA was extracted using the QIAGEN
204 Genomic DNA kit and QIAGEN Genomic-tip20/G, according to the manufacturer's instructions.
205 Sequencing libraries were prepared by SeqCenter (Pittsburgh, PA) using the Illumina DNA Prep kit and
206 sequenced on an Illumina NovaSeq 6000. The genome sequences and GFF annotation files for the
207 SC5314 reference genome (haplotype A, A22-s07-m01-r130) were downloaded from the *Candida*
208 Genome Database (Braun et al. 2005; Inglis et al. 2012) (http://www.candidagenome.org/). Reads were
209 aligned to the reference genome using Minimap2 v2.17 (Li 2018). Sequence Alignment/Map tools
210 (SAMtools) v1.10 (r783) (Li et al. 2009) and Picard tools v2.23.3 (http://broadinstitute.github.io/picard)
211 were used to filter, sort, and convert the SAM files. Coverage levels were calculated using GATK
212 (McKenna et al. 2010). To estimate chromosome copy numbers, the read alignment depth was
213 calculated for 1 kbp windows across each genome and normalized to the average depth per genome.
214 For published genomes, sequence information is included in **Supplementary Table 1**. Sequence read
215 data for all other genomes have been deposited in the NCBI Sequence Read Archive under BioProject ID
216 PRJNA1354400.
217
218 **Results**
219 **Design of a 16-plex chromosome-arm panel using six-color combinations.** To quantify the eight
220 *C. albicans* chromosomes, we developed a 16-plex ddPCR assay targeting one locus on each
221 chromosome arm (**Fig. 1A**). The assay employs 6 fluorophores and assigns each chromosome
222 arm/target a unique single- or dual-color code (Santos-Barriopedro 2023) (**Supplementary Table 3**),
223 allowing all 16 loci to be resolved within a single reaction using simple per-channel thresholding.
224 Detection relies on Flex Probe chemistry: target-specific Flex Probes are non-fluorescent
225 oligonucleotides that, upon target amplification, release a universal tag (Tag-oligo) that hybridizes to a

226 fluorophore-labeled Universal Reporter and is extended, generating the fluorescence signal used for
227 droplet calling (**Fig. 1B**).
228 Candidate loci were selected based on normalized WGS coverage near diploid levels at the
229 target site, proximity to the centromere (to avoid telomeric regions prone to mutation and loss of
230 heterozygosity), and association with essential or housekeeping functions (to reduce the likelihood of
231 sequence divergence or structural variation that could impair probe binding). The resulting 16 targets
232 (**Fig. 1C**) provide balanced chromosomal coverage and, because they were chosen from conserved
233 regions, are expected to support consistent probe binding across genetically diverse isolates. As an
234 initial performance check independent of strain background, we tested the panel using equimolar
235 synthetic double-stranded DNA controls (gBlocks) for each chromosome arm. Under these controlled
236 conditions, the measured arm ratios were close to the expected value of 1, supporting the accuracy of
237 the target set and color-coding scheme. Together, this design establishes a scalable, single-reaction
238 framework for genome-wide chromosome copy-number measurement in *C. albicans*.
239
240 **Probe redesign and PCR optimization improve multiplex cluster separation.** Probes were initially
241 designed as non-competing dual Flex Probe pairs, in which two differently labeled probes bind adjacent
242 sites within the same amplicon (Santos-Barriopedro 2023). Each target was first evaluated individually
243 (simplex) and then combined into the full multiplex panel for single-reaction detection of all 16 loci.
244 When tested on genomic DNA, simplex analysis of two strains (SC5314 (euploid A) and CAY8836-SC (Chr
245 1,4,5,7 3X)) revealed reproducible deviations from the expected R:L ratio for a subset of chromosomes:
246 Chr1, Chr4, and Chr6 in SC5314, and Chr4 and Chr6 in CAY8836-SC (**Supplementary Fig. 2A**). These
247 deviations persisted in multiplex runs, and an additional imbalance was observed for ChrR in both
248 strains (**Supplementary Fig. 2A**). Inspection of 2D amplitude (dot) plots from simplex reactions
249 localized these effects to probe performance. For SC5314, only one of the two probes designed for each

250 arm produced efficient binding for Chr1, Chr4, and Chr6, whereas in CAY8836-SC, this behavior was
251 restricted to Chr4 and Chr6 (**Supplementary Fig. 2B**).

252 Because each arm should contribute ~50% of the double-positive signal, inefficient detection of
253 one arm depletes the double-positive cluster and inflates single-color droplets, yielding an apparent
254 arm imbalance. Notably, ChrRL is the only target encoded in a single channel (IR), and Chr6R generated
255 a marked excess of IR-only droplets (**Supplementary Table 5**). Thus, a fraction of Chr6R molecules that
256 should have contributed to the double-positive population were instead detected only in IR, biasing the
257 inferred ChrR R:L ratio. We hypothesized that single-nucleotide polymorphisms (SNPs) and/or local DNA
258 conformation impaired probe hybridization. To correct these probe-specific biases, we redesigned the
259 probes for Chr1L, Chr4R, and Chr6R using a competing dual Flex Probe configuration, in which both
260 probes target the same region and compete for hybridization (Santos-Barriopedro 2023). For each
261 target, the redesigned pair was based on the better-performing sequence from the original non-
262 competing design.

263 Additional optimization steps included increasing the probe concentration from 0.5 µM to 1 µM
264 and extending the final elongation step from 10 to 15 min. These adjustments increased signal
265 amplitude and reduced stochastic detection variability, particularly under multiplex conditions.
266 Consistent with this, average separability scores (indicating how well the positive and negative
267 distributions are separated, **Supplementary Fig. 1**) improved after probe redesign and reaction
268 optimization, yielding well-resolved positive and negative droplet populations across all targets. The
269 longer final elongation improved separability (**Supplementary Fig. 3A**), likely by allowing additional
270 time for the Tag-oligo hybridized to the Universal Reporter to elongate and release the fluorophore.
271 Because the optimal elongation time is assay-dependent, it can be adjusted to improve amplification
272 efficacy and maximize cluster height, although overly long elongation steps may occasionally produce
273 low-level positive droplets in the no-template control.

274 Together, these refinements produced distinct, non-overlapping signal clusters for all 16 loci
275 within a single ddPCR reaction. Partition clustering analysis reliably separated positive and negative
276 droplets, enabling direct absolute quantification of each target and robust genome-wide aneuploidy
277 measurement in *C. albicans*.
278
279 **Spillover compensation improves multiplex droplet calling.** Droplet calling and quantification were
280 performed in Crystal Miner. Because the naica system detects six fluorophores across six channels,
281 partial spectral overlap ("spillover") can distort droplet amplitudes and bias multiplex quantification.
282 Although each fluorophore is primarily excited and detected in its own channel, low-level excitation by
283 other light sources and broad emission spectra can introduce measurable signal into non-primary
284 channels. To correct this, we generated an assay-specific spillover compensation matrix using chambers
285 containing single-color probe sets. For each fluorophore, we quantified the fraction of its signal
286 detected in the other channels and used these values to build a spillover compensation matrix. The
287 matrix was then inverted and applied to raw fluorescence measurements to obtain spillover-corrected
288 fluorophore intensities and adjusted for background fluorescence. This correction yielded cleaner one-
289 dimensional amplitude distributions for thresholding (**Supplementary Fig. 3B**) and restored the
290 orthogonal cluster geometry in 2D amplitude plots, improving separation between negative and
291 positive droplet populations (**Supplementary Fig. 3C**). The resulting matrix can be saved and reused
292 for all runs performed with this assay. After compensation, thresholds separating positive and negative
293 droplets were manually set in each channel, and the population editor was used to define single- and
294 dual-color codes for positive droplets of each target (e.g., *CCT2* in the blue and green channels and *SSK2*
295 in the teal and yellow channels, **Supplementary Fig. 3C**). Using Poisson statistics, the software then
296 estimated target concentrations and reported confidence intervals. Together, spillover correction and
297 consistent droplet calling across runs improve high-order multiplex quantification.

298

299 **Column-based DNA extraction and higher DNA input improve 16-plex copy number accuracy.** To
300 assess how genomic DNA preparation affects copy-number calling, we compared a widely used phenol–
301 chloroform protocol with a commercial column-based kit (QIAGEN) across five *C. albicans* isolates
302 spanning euploid (SC5314), simple aneuploid (Chr3 1X, ChrR 3X), and complex aneuploid (Chr3,6 3X,
303 Chr6,R 4X) karyotypes. Baseline chromosome copy numbers were first established by Illumina WGS (**Fig.**
304 **2A**). When these samples were analyzed with the 16-plex ddPCR assay, phenol–chloroform DNA
305 produced noisier copy-number profiles and frequent deviations from the WGS karyotype (**Fig. 2B**). In
306 contrast, column-purified DNA yielded chromosome copy-number estimates that closely matched WGS
307 across all isolates (**Fig. 2B**), reduced technical variance (from a mean SD of 0.71 to 0.38), and increased
308 the fraction of positive droplets per reaction (from a total of 3.25% to 21.21%) (**Supplementary Fig. 4**).
309 We next asked whether increasing DNA input could further improve assay precision. While 10
310 pg/µL of column-purified DNA produced acceptable profiles, raising the input to 30 pg/µL increased
311 concordance with WGS (**Fig. 2B**), improved reproducibility across replicates (from a mean SD of 0.38 to
312 0.16), and further increased the positive droplet fraction from 21.21% to 38.7% (**Supplementary Fig. 4**).
313 Based on these results, the optimized workflow uses 30 pg of column-purified gDNA per 5 µL reaction to
314 maximize target detection and minimize false aneuploid calls.

315

316 **DNA digestion increases droplet resolution and copy number accuracy in the 16-plex assay.** High-
317 molecular-weight genomic DNA can interfere with droplet formation and reduce amplification
318 uniformity across targets. To test whether template fragmentation enhances assay performance,
319 genomic DNA from the euploid reference strain SC5314 (euploid A) was digested with EcoRI, BamHI,
320 HindIII, or PstI, either individually or in pairwise combinations, before amplification. Enzymes were
321 selected to avoid predicted cut sites within the 16 amplicons (**Supplementary Table 2**).

322 Across conditions, digestion improved the accuracy of chromosome copy-number estimates
323 relative to undigested DNA (**Fig. 2C**). While single-enzyme digests provided modest gains, enzyme
324 combinations produced the most consistent improvements, particularly when PstI was combined with
325 either EcoRI or HindIII. This was reflected by reduced variability between replicates in copy-number
326 estimates and higher separability scores across chromosome arms (**Supplementary Fig. 5A-B**).
327 Digestion also increased the fraction of positive droplets (**Supplementary Fig. 5C**), consistent with
328 improved accessibility of amplifiable templates and reduced stochastic dropout. Undigested DNA
329 tended to overestimate copy number for specific chromosomes, particularly for Chr1 and Chr4, whereas
330 digestion corrected these biases and returned copy numbers closer to the expected disomic baseline
331 (**Fig. 2C** and **Supplementary Fig. 5D**). Taken together, restriction digestion improved both droplet
332 cluster resolution and quantitative accuracy. Consequently, we incorporated DNA pre-digestion with
333 PstI+HindIII as a standard step in the optimized 16-plex workflow.
334
335 **The 16-plex assay sensitively detects mosaic aneuploidy and matches WGS across diverse**
336 **karyotypes.** To test sensitivity for detecting emerging aneuploid subpopulations, we generated defined
337 mixtures of disomic and trisomic cultures from the same strain background (ChrR 2X:3X) at 25%, 50%,
338 and 75% trisomic fractions. The assay revealed a progressive increase in ChrR copy number that closely
339 matched the expected mixture averages, and reliably distinguished trisomy when only 25% of the
340 population carried the extra chromosome (**Fig. 3A**). The same trend was observed at the chromosome-
341 arm level for RL and RR (**Supplementary Table 6**), indicating that the 16-plex format can resolve mosaic
342 aneuploidy at low abundance despite the sampling noise inherent to droplet partitioning.
343 We next assessed species specificity using genomic DNA from *C. dubliniensis* and *C. tropicalis*.
344 Under standard cycling conditions, none of the 16 targets generated positive droplets, supporting assay

345 specificity for *C. albicans* and suggesting that detection of related species would require redesigned
346 primers/probes.

347 Finally, we benchmarked ddPCR copy-number estimates against Illumina WGS across a panel
348 spanning euploid isolates and increasingly complex aneuploid karyotypes (**Fig. 3B**). Euploid controls
349 clustered tightly around the expected disomic baseline, and the assay correctly identified single-
350 chromosome aneuploidies across all eight chromosomes, including Chr3 monosomy and distinct
351 trisomies (**Fig. 3C**). Isolates carrying two supernumerary chromosomes were also called accurately, with
352 strong agreement between ddPCR and WGS (**Fig. 3B-C**) and consistent left/right arm estimates
353 (**Supplementary Table 7**). In highly aneuploid isolates (≥4 altered chromosomes), ddPCR still captured
354 broad copy-number elevations and flagged complex karyotypes, but complete resolution became less
355 consistent, occasionally underestimating one affected chromosome, likely because calling becomes
356 more challenging when many targets shift at once in highly aneuploid genomes (**Fig. 3C**).

357 Overall, these results show that the 16-plex ddPCR assay provides WGS-concordant copy-
358 number calls for euploid, single-, and dual-aneuploid karyotypes, while remaining sensitive enough to
359 detect low-frequency trisomic subclones and to flag isolates with more complex chromosomal
360 alterations.

361

362 **Discussion**

363 Here, we developed and validated a 16-plex ddPCR assay for genome-wide chromosome copy-
364 number measurement in *C. albicans.* The assay combines digital quantification with high-order
365 multiplexing through color-combination encoding across six fluorescence channels, enabling
366 simultaneous readout of all 16 chromosome arms in a single reaction. Targeting both chromosome arms
367 gives a built-in cross-check (left vs. right) and helps capture large arm-scale copy-number changes that
368 single-locus qPCR assays can miss. In practice, this workflow provides a rapid alternative to sequencing:

369 from gDNA to copy-number calls can be completed within a day, without library preparation or
370 bioinformatics.

371 As with any targeted assay, performance depends on the complementarity between probe and
372 template. Locus-specific polymorphisms or small indels in primer/probe binding sites can reduce
373 hybridization efficiency and bias local quantification in genetically divergent isolates. In addition, the
374 resolution is limited to the assayed loci: partial aneuploidies that do not include the selected target
375 region will not be detected, and breakpoints cannot be mapped. Finally, high-order multiplexing
376 requires stable fluorescence calibration. Spectral overlap and variability between replicates can affect
377 cluster positions if compensation and thresholding are not standardized. These limitations can be
378 mitigated by (i) selecting conserved targets (as done here) and redesigning individual probe sets when
379 strain-specific dropout is observed, (ii) including a reference strain with a known karyotype, and (iii)
380 using fixed instrument templates and a fixed spillover compensation matrix to stabilize cluster
381 geometry across experiments.

382 Across a diverse isolate panel, the 16-plex assay showed strong agreement with WGS for euploid
383 strains and for isolates carrying 1-3 supernumerary chromosomes, and it sensitively detected mosaic
384 trisomy down to 25% abundance in mixed populations. Performance was less consistent in highly
385 aneuploid genomes, where many chromosomes deviate simultaneously and accurate calling becomes
386 more challenging. Nevertheless, even in these cases, the assay reliably flagged complex karyotypes and
387 captured broad patterns of copy-number variation. Together, these results define a practical operating
388 range: highly accurate for simple aneuploid states, and informative for more complex karyotypes where
389 follow-up by WGS may be warranted.

390 Relative to WGS, ddPCR offers advantages in speed, cost, and sample requirements. It is best
391 suited for large-scale screening experiments where many isolates must be profiled quickly, as well as
392 for settings where sequencing infrastructure is limited. The assay's reliance on droplet partitioning also

393 makes it compatible with low DNA inputs and heterogeneous populations, making it relevant for clinical
394 isolates and samples where aneuploid subpopulations may be emerging. Our optimization results
395 underscore, however, that standardized sample preparation is essential: column-based extraction,
396 higher DNA input, and restriction digestion substantially improved positive droplet fraction, cluster
397 separation, and copy-number accuracy.

398 A key strength of the assay is its modularity. Because multiplex structure is encoded by probe
399 sequences and fluorophore combinations, panels can be reconfigured to address new biological
400 questions without changing the underlying workflow. For example, the same design principles could be
401 extended to track recurrent aneuploidies linked to drug resistance or adaptation, to include loci
402 reporting focal amplifications, or to incorporate species- or clade-informative markers alongside copy-
403 number targets. More broadly, by redesigning primer/probe sequences while preserving the color-
404 combination logic, this approach should translate to other fungal species where copy number variation
405 contributes to stress resistance and host adaptation.

406 Overall, this 16-plex ddPCR assay bridges a practical gap between comprehensive but resource-
407 intensive sequencing and low-multiplex assays. It provides an accessible platform for quantitative
408 monitoring of genome instability, enabling rapid, scalable readout of karyotypic variation in both
409 experimental and clinical contexts.

410

411 **Data availability.** Sequence read data generated in this study have been deposited in the NCBI
412 Sequence Read Archive under BioProject PRJNA1354400. Accession information for previously
413 published genomes analyzed here is provided in **Supplementary Table 1**. Strains are available upon
414 request. The authors affirm that all data necessary for confirming the conclusions of the article are
415 present within the article, figures, and tables.

416

Acknowledgements. We thank members of the Fungal Heterogeneity Group for helpful discussions.

Study Funding. This work was supported by the FRM Espoirs de la Recherche Postdoctoral Fellowship (EIM), the Pasteur Roux-Cantarini Fellowship (PB), ANR GENOMEHET (IVE), PTR Carnot Pasteur (IVE), and the Institut Pasteur.

Conflict of Interest. SU, SAS, SR, CJ, and LP are employees of Bio-Rad Laboratories, Inc. (Life Science Group, Villejuif, France). All other authors declare no competing interests.

Figure Legends

Figure 1. Assay design and fluorescence encoding strategy for 16-plex ddPCR chromosome copy-number profiling in *C. albicans*. (A) Overview of the experimental workflow, including overnight growth of cells (liquid or solid culture), genomic DNA extraction, restriction-enzyme digestion, reaction mix preparation, droplet digital PCR, and downstream data analysis. (B) Flex Probe/Universal Reporter detection chemistry underlying the multiplexing strategy. Forward and reverse primers (gray arrows), Flex probes (gray lines), universal reporters, and genomic DNA are combined in a single reaction. During amplification, target-specific Flex probes are hydrolyzed to release a universal tag (Tag-oligo) that hybridizes to a fluorophore-labeled Universal Reporter. Subsequent elongation generates the target-specific fluorescence signal used for droplet calling, enabling simultaneous discrimination of all 16 loci. (C) Schematic of the eight *C. albicans* chromosomes showing the positions of the 16 targeted loci (one per chromosome arm). Centromeres and major repeat sequence (MRS) regions are indicated. Each arm is assigned a unique single- or dual-color code across six fluorescence channels to enable multiplex detection within a single reaction.

441 **Figure 2.** Genomic DNA preparation steps that improve 16-plex ddPCR accuracy. (A) Whole-genome
442 sequencing-derived chromosome copy-number profiles for a panel comprising one euploid reference
443 isolate and four aneuploid isolates representing simple and complex karyotypes. Values are shown as
444 chromosome-level copy numbers. (B) Heatmaps of ddPCR-derived chromosome copy-number
445 estimates for the same isolates under different extraction/input conditions, comparing phenol–
446 chloroform extraction (10 pg/µL input) to column-based purification (QIAGEN; 10 pg/µL and 30 pg/µL
447 input). (C) Effect of restriction-enzyme digestion on ddPCR accuracy using the euploid reference strain
448 SC5314 (euploid A). Heatmaps show chromosome copy-number estimates obtained without digestion
449 (none) or after digestion with individual enzymes or enzyme combinations.
450
451 **Figure 3.** Assay performance across mixed populations and diverse isolate karyotypes. (A) Detection of
452 mosaic aneuploidy using defined mixtures of disomic (euploid B, ChrR 2X) and aneuploid (ChrR 3X)
453 subpopulations. (B) WGS-based chromosome copy-number profiles for 24 isolates spanning euploid,
454 single-aneuploid, and complex karyotypes. (C) Corresponding ddPCR-based chromosome copy-
455 number estimates for the same isolate panel.
456
457 **Supplementary Figure Legends**
458 **Supplementary Figure 1.** Separability score used to quantify droplet-cluster resolution. Definition of
459 the separability score (S) computed from the mean and dispersion of positive and negative droplet
460 amplitude distributions and the number of droplets in each population. Higher values indicate better
461 separation between positive and negative droplets and improved robustness of thresholding.
462
463 **Supplementary Figure 2.** Strain-dependent chromosome arm imbalances reveal probe-specific
464 underperformance. (A) Heatmap of chromosome arm R:L ratios for isolates SC5314 (euploid A) and

465 CAY8836-SC (Chr1,4,5,7, 3X) measured in simplex and multiplex. For each chromosome, the ratio was
466 calculated as the copy-number estimate for the right-arm (R) target divided by the left-arm (L) target;
467 values near 1 indicate balanced detection of both arms, whereas deviations reflect arm-specific bias
468 (notably for Chr1, Chr4, Chr6, and ChrR). (B) Representative 2D amplitude (dot) plots from simplex
469 reactions for arm targets showing the underlying probe behavior in euploid A (top) and Chr1,4,5,7, 3X
470 (bottom) isolates. For Chr1L, Chr4R, and Chr6R, one probe in the original non-competing dual-probe
471 pair yields inefficient detection (shown by the crossed-out probe), reducing the expected double-
472 positive population and inflating single-color droplets. In contrast, the corresponding partner-arm
473 targets (Chr1R, Chr4L, Chr6L) show the expected well-separated positive clusters in their assigned
474 channel pairs.
475
476 **Supplementary Figure 3.** Final elongation time and spillover compensation improve cluster separation
477 in multiplex reactions. (A) Heatmap of separability scores for each chromosome-arm target (columns)
478 across representative isolates, comparing a 10 min versus 15 min final elongation step. Higher scores
479 indicate better separation between positive and negative droplet populations. (B) Representative 1D
480 amplitude plots in the yellow and green channels before and after applying spillover compensation.
481 Compensation yields a cleaner separation of positive (colored) and negative (gray) droplet populations.
482 (C) Representative 2D amplitude (dot) plots (Blue vs Green; Teal vs Yellow) before and after
483 compensation. Spillover correction restores the expected cluster geometry and increases separation
484 between negative (gray) and positive (colored) droplet populations, supporting more reliable droplet
485 calling.
486
487 **Supplementary Figure 4.** Effects of DNA extraction method and DNA input amount on the performance
488 of the 16-plex assay across euploid and aneuploid isolates. (A) Standard deviation of chromosome copy-

489 number estimates across biological replicates as a measure of technical variance. (B) Fraction of
490 positive droplets per reaction/condition, reflecting effective amplifiable template availability. (C)
491 Chromosome copy-number estimates under each condition, highlighting false-positive calls under
492 suboptimal preparation.
493
494 **Supplementary Figure 5.** Restriction-enzyme digestion improves droplet resolution and assay
495 consistency. Performance metrics for undigested DNA versus digestion with single enzymes or enzyme
496 combinations. Heatmaps summarize changes following SC5314 (euploid A) DNA digestion in (A)
497 variability of chromosome copy-number estimates (SD across replicates), (B) droplet separability
498 scores, (C) fraction of positive droplets, and (D) chromosome copy-number profiles.
499
500 **Supplementary Table Legends**
501 **Supplementary Table 1**. *Candida* isolates used in this study. List of isolates analyzed, including strain
502 names and aliases, sequence information, and literature references where applicable.
503
504 **Supplementary Table 2.** Panel of restriction enzymes evaluated for genomic DNA digestion and their
505 predicted cleavage within the amplified target region of each chromosome arm.
506
507 **Supplementary Table 3.** Target loci and fluorophore combinations used in the 16-plex ddPCR assay.
508 Each *C. albicans* chromosome arm is represented by a single target gene detected through a unique
509 fluorophore or pair of fluorophores across six color channels. The combination of fluorophores defines
510 a distinct fluorescence signature for each target. The final column indicates whether the two probes for
511 that target were designed with competitive or non-competitive binding.
512

513 **Supplementary Table 4.** Primers and Flex probes used in this study.

514

515 **Supplementary Table 5.** Percentage of target detection for each chromosome arm for strains SC5314
516 (euploid A) and CAY8836-SC (Chr 1,4,5,7 3X), calculated by dividing the number of positive droplets per
517 arm by the total number of droplets for each chromosome.

518

519 **Supplementary Table 6.** Chromosome-arm copy number estimates in defined mixed populations of
520 euploid B (ChrR disomic, 2X) and ChrR 3X (ChrR trisomic, 3X) isolates from the same genetic background
521 (CAY6440) at 0%, 25%, 50%, 75%, and 100% trisomic fractions.

522

523 **Supplementary Table 7.** Chromosome-arm copy number estimates across a panel of 24 isolates,
524 showing concordance between left and right arms for most chromosomes and highlighting isolates
525 where arm estimates diverge, consistent with arm-biased copy-number changes or structural variation
526 spanning one target.

527

528 **References**

529 Bennett, R.J., A. Forche, and J. Berman, 2014 Rapid mechanisms for generating genome diversity: whole
530 ploidy shifts, aneuploidy, and loss of heterozygosity. *Cold Spring Harb Perspect Med* 4 (10).

531 Braun, B.R., M. van Het Hoog, C. d'Enfert, M. Martchenko, J. Dungan *et al.*, 2005 A human-curated
532 annotation of the *Candida albicans* genome. *PLoS Genet* 1 (1):36-57.

533 Brown, G.D., D.W. Denning, N.A. Gow, S.M. Levitz, M.G. Netea *et al.*, 2012 Hidden killers: human fungal
534 infections. *Sci Transl Med* 4 (165):165rv113.

535 Denning, D.W., 2024 Global incidence and mortality of severe fungal disease. *Lancet Infect Dis*.
536 Jul;24(7):e428-e438.
537 Ene, I.V., and R.J. Bennett, 2014 The cryptic sexual strategies of human fungal pathogens. *Nat Rev*
538 *Microbiol* 12 (4):239-251.
539 Ene, I.V., R.A. Farrer, M.P. Hirakawa, K. Agwamba, C.A. Cuomo *et al.*, 2018 Global analysis of mutations
540 driving microevolution of a heterozygous diploid fungal pathogen. *Proc Natl Acad Sci U S A*.
541 Forche, A., 2014 Large-Scale Chromosomal Changes and Associated Fitness Consequences in
542 Pathogenic Fungi. *Curr Fungal Infect Rep* 8 (2):163-170.
543 Forche, A., G. Cromie, A.C. Gerstein, N.V. Solis, T. Pisithkul *et al.*, 2018 Rapid Phenotypic and Genotypic
544 Diversification After Exposure to the Oral Host Niche in *Candida albicans*. *Genetics* 209 (3):725-741.
545 Inglis, D.O., M.B. Arnaud, J. Binkley, P. Shah, M.S. Skrzypek *et al.*, 2012 The *Candida* genome database
546 incorporates multiple *Candida* species: multispecies search and analysis tools with curated gene and
547 protein information for *Candida albicans* and *Candida glabrata*. *Nucleic acids research* 40 (Database
548 issue):D667-674.
549 Kakade, P., S. Sircaik, C. Maufrais, I.V. Ene, and R.J. Bennett, 2023 Aneuploidy and gene dosage regulate
550 filamentation and host colonization by *Candida albicans. Proc Natl Acad Sci U S A* 120
551 (11):e2218163120.
552 Li, H., 2018 Minimap2: pairwise alignment for nucleotide sequences. *Bioinformatics* 34 (18):3094-3100.
553 Li, H., B. Handsaker, A. Wysoker, T. Fennell, J. Ruan *et al.*, 2009 The Sequence Alignment/Map format
554 and SAMtools. *Bioinformatics* 25 (16):2078-2079.
555 Li, R., and J. Zhu, 2022 Effects of aneuploidy on cell behaviour and function. *Nat Rev Mol Cell Biol* 23
556 (4):250-265.
557 Madic, J., A. Zocevic, V. Senlis, E. Fradet, B. Andre *et al.*, 2016 Three-color crystal digital PCR. *Biomol*
558 *Detect Quantif* 10:34-46.

559 McKenna, A., M. Hanna, E. Banks, A. Sivachenko, K. Cibulskis *et al.*, 2010 The Genome Analysis Toolkit: a
560 MapReduce framework for analyzing next-generation DNA sequencing data. *Genome Res* 20 (9):1297-
561 1303.
562 Morrow, C.A., and J.A. Fraser, 2013 Ploidy variation as an adaptive mechanism in human pathogenic
563 fungi. *Seminars in cell & developmental biology* 24 (4):339-346.
564 Pappas, P.G., M.S. Lionakis, M.C. Arendrup, L. Ostrosky-Zeichner, and B.J. Kullberg, 2018 Invasive
565 candidiasis. *Nat Rev Dis Primers* 4:18026.
566 Santos-Barriopedro, I., Ursuegui, S., Fradet, E., Dangla, R., 2023 Robust higher-order multiplexing in
567 digital PCR by color-combination. *bioRxiv*. doi: 10.1101/2023.05.10.540190.
568 Selmecki, A., A. Forche, and J. Berman, 2006 Aneuploidy and isochromosome formation in drug-
569 resistant *Candida albicans*. *Science (New York, N.Y.)* 313 (5785):367-370.
570 Selmecki, A., A. Forche, and J. Berman, 2010 Genomic plasticity of the human fungal pathogen *Candida*
571 *albicans*. *Eukaryot Cell* 9 (7):991-1008.
572 Selmecki, A., M. Gerami-Nejad, C. Paulson, A. Forche, and J. Berman, 2008 An isochromosome confers
573 drug resistance *in vivo* by amplification of two genes, *ERG11* and *TAC1*. *Molecular microbiology* 68
574 (3):624-641.
575 Todd, R.T., and A. Selmecki, 2020 Expandable and reversible copy number amplification drives rapid
576 adaptation to antifungal drugs. *Elife* 9.
577 Todd, R.T., T.D. Wikoff, A. Forche, and A. Selmecki, 2019 Genome plasticity in *Candida albicans* is driven
578 by long repeat sequences. *Elife* 8.
579 Torres, E.M., T. Sokolsky, C.M. Tucker, L.Y. Chan, M. Boselli *et al.*, 2007 Effects of aneuploidy on cellular
580 physiology and cell division in haploid yeast. *Science (New York, N.Y.)* 317 (5840):916-924.
581 Torres, E.M., B.R. Williams, and A. Amon, 2008 Aneuploidy: cells losing their balance. *Genetics* 179
582 (2):737-746.

583 Tsai, H.J., and A. Nelliat, 2019 A Double-Edged Sword: Aneuploidy is a Prevalent Strategy in Fungal
584 Adaptation. *Genes (Basel)* 10 (10).
585 Tsai, H.J., A.R. Nelliat, M.I. Choudhury, A. Kucharavy, W.D. Bradford *et al.*, 2019 Hypo-osmotic-like stress
586 underlies general cellular defects of aneuploidy. *Nature* 570 (7759):117-121.
587 Vande Zande, P., X. Zhou, and A. Selmecki, 2023 The Dynamic Fungal Genome: Polyploidy, Aneuploidy
588 and Copy Number Variation in Response to Stress. *Annu Rev Microbiol* 77:341-361.
589 Vasudevan, A., K.M. Schukken, E.L. Sausville, V. Girish, O.A. Adebambo *et al.*, 2021 Aneuploidy as a
590 promoter and suppressor of malignant growth. *Nat Rev Cancer* 21 (2):89-103.
591 Yang, F., V. Gritsenko, Y. Slor Futterman, L. Gao, C. Zhen *et al.*, 2021a Tunicamycin Potentiates Antifungal
592 Drug Tolerance via Aneuploidy in *Candida albicans*. *MBio* 12 (4):e0227221.
593 Yang, F., F. Teoh, A.S.M. Tan, Y. Cao, N. Pavelka *et al.*, 2019 Aneuploidy Enables Cross-Adaptation to
594 Unrelated Drugs. *Mol Biol Evol* 36 (8):1768-1782.
595 Yang, F., R.T. Todd, A. Selmecki, Y.Y. Jiang, Y.B. Cao *et al.*, 2021b The fitness costs and benefits of trisomy
596 of each *Candida albicans* chromosome. *Genetics* 218 (2).
597 Zhu, J., H.J. Tsai, M.R. Gordon, and R. Li, 2018 Cellular Stress Associated with Aneuploidy. *Dev Cell* 44
598 (4):420-431.
599

Figure 1

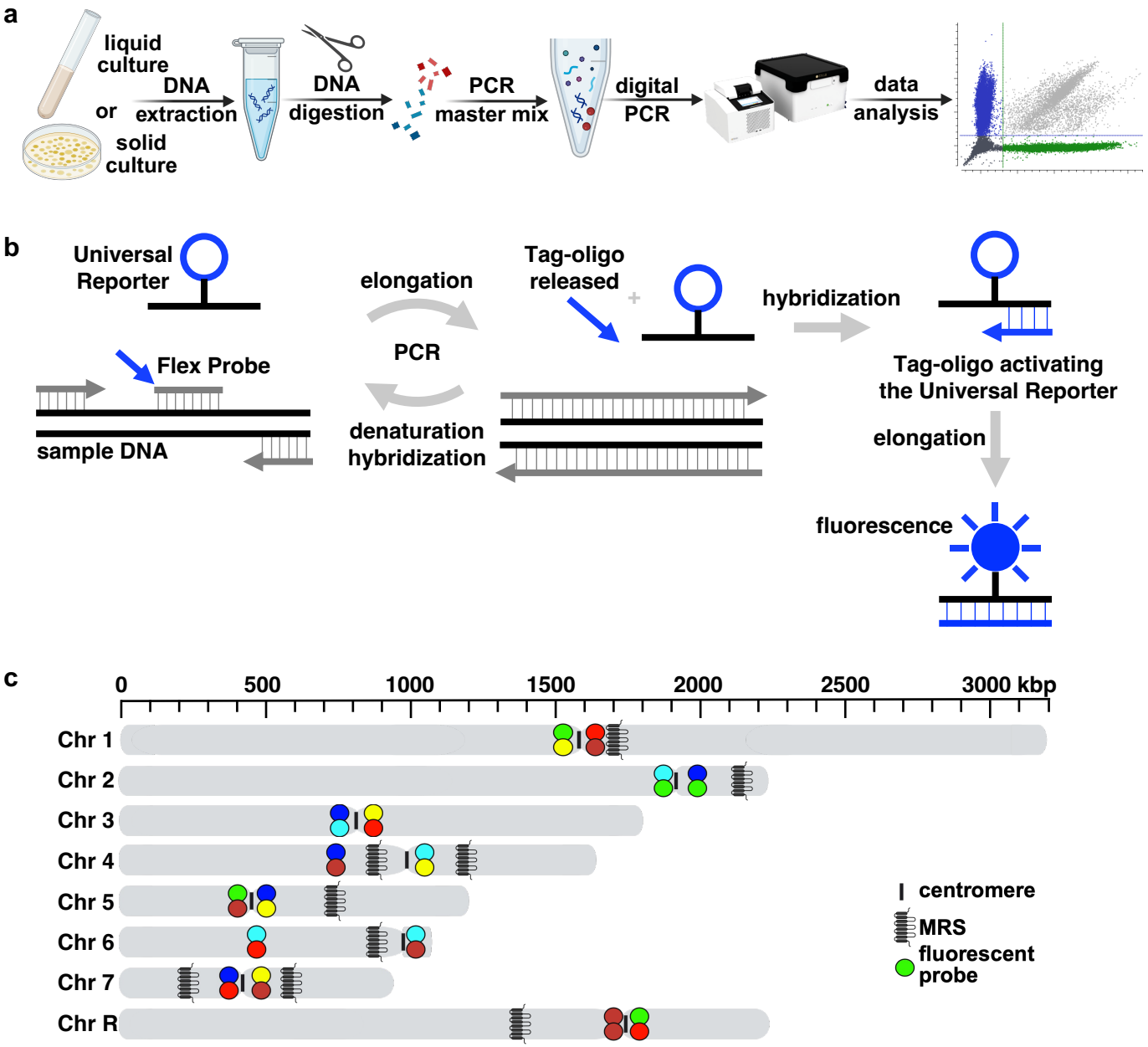
a
liquid culture
or
solid culture
DNA extraction
DNA digestion
PCR master mix
digital PCR
data analysis
b
Universal Reporter
Flex Probe
sample DNA
elongation
PCR
denaturation hybridization
Tag-oligo released
hybridization
Tag-oligo activating the Universal Reporter
elongation
fluorescence
c
0
500
1000
1500
2000
2500
3000 kbp
Chr 1
Chr 2
Chr 3
Chr 4
Chr 5
Chr 6
Chr 7
Chr R
centromere
MRS
fluorescent probe

Figure 2

a

		Chromosome							
		1	2	3	4	5	6	7	R
WGS	euploid A	2.00	2.00	2.10	2.00	2.00	2.00	2.10	2.00
	Chr3 1X	2.00	1.98	1.08	2.24	1.96	1.94	2.00	2.02
	ChrR 3X	2.00	2.00	2.10	2.00	2.00	2.00	2.10	2.80
	Chr3,6 3X	1.90	1.90	3.00	2.00	2.00	2.90	2.20	1.90
	Chr6,R 4X	2.85	2.85	3.00	2.85	2.79	3.69	3.09	3.75

Chromosome copy number

1 2 3

b

		Chromosome							
		1	2	3	4	5	6	7	R
phenol chloroform 10 pg	euploid A	1.69	2.13	1.81	2.82	2.10	1.85	1.54	3.00
	Chr3 1X	2.37	2.03	1.48	2.37	2.23	1.02	2.89	2.12
	ChrR 3X	1.91	2.16	1.73	2.09	2.50	2.27	1.43	2.61
	Chr3,6 3X	1.46	2.12	2.67	2.75	1.90	2.20	1.67	2.21
	Chr6,R 4X	2.30	2.89	1.34	3.12	3.50	4.44	1.96	4.31
Qiagen 10 pg	euploid A	1.95	2.04	2.06	1.93	1.98	2.13	2.03	1.90
	Chr3 1X	2.05	2.22	1.32	2.01	2.07	2.20	1.95	2.27
	ChrR 3X	1.93	2.02	1.88	1.77	2.15	1.85	2.11	2.97
	Chr3,6 3X	1.85	2.05	3.05	1.90	1.86	2.95	2.03	1.85
	Chr6,R 4X	3.44	3.35	2.74	2.86	1.96	3.88	2.82	4.17
Qiagen 30 pg	euploid A	2.08	2.00	1.92	1.99	1.89	2.04	2.02	2.10
	Chr3 1X	2.01	2.05	1.06	2.37	1.87	1.98	2.07	2.03
	ChrR 3X	2.13	2.16	1.93	2.00	1.89	2.00	1.89	3.04
	Chr3,6 3X	1.92	2.03	2.83	1.96	1.91	2.93	1.94	2.12
	Chr6,R 4X	3.07	3.03	2.81	3.09	2.82	3.77	2.69	4.16

Chromosome copy number

1 2 3

c

	Chromosome							
	1	2	3	4	5	6	7	R
none	2.47	2.14	1.99	2.26	1.78	1.86	1.99	1.88
EcoRI	2.01	2.06	2.03	2.01	2.05	1.97	2.02	1.92
BamHI	1.95	1.69	2.02	2.21	2.09	1.95	2.09	2.07
HindIII	1.85	2.11	2.03	2.18	1.83	1.90	1.93	1.99
PstI	1.98	1.95	1.93	1.92	2.01	1.93	2.26	2.07
PstI+BamHI	1.82	2.07	2.00	2.07	1.93	1.93	2.08	1.98
PstI+EcoRI	2.09	1.96	1.93	2.04	2.01	2.15	2.01	1.95
PstI+HindIII	1.95	2.04	2.06	1.93	1.98	2.13	2.03	1.90
BamHI+EcoRI	1.89	2.09	1.99	2.08	1.94	2.08	2.08	1.97
BamHI+HindIII	1.92	2.25	1.98	2.02	1.97	2.04	2.06	1.96
HindIII+EcoRI	1.99	2.05	1.95	2.07	2.15	2.07	2.02	1.98

Chromosome copy number

1 2 3

Figure 3

a

ChrR 2X:3X	Chromosome 1	2	3	4	5	6	7	R
100:0	2.02	2.02	2.01	1.94	2.04	2.07	1.97	1.91
75:25	1.99	2.02	1.89	1.95	2.06	1.94	1.85	2.28
50:50	1.94	1.99	2.07	2.04	1.94	1.91	1.97	2.47
25:75	2.01	2.03	1.89	2.00	1.94	1.90	1.91	2.67
0:100	2.06	1.92	1.97	2.01	1.96	2.06	1.86	2.97

Chromosome copy number

1 2 3

b Whole genome sequencing

	Chromosome 1	2	3	4	5	6	7	R
euploid A	1.96	1.94	2.06	2.00	2.00	2.02	2.08	1.98
euploid B	2.00	1.98	2.10	2.00	1.98	1.98	2.10	2.00
euploid C	1.94	1.98	2.12	1.94	1.90	2.02	2.06	2.00
euploid D	2.02	2.00	2.06	2.00	1.98	2.00	1.96	2.04
euploid E	1.96	1.96	2.04	1.98	2.14	2.00	2.18	1.94
Chr3 1X	2.00	1.98	1.08	2.24	1.96	1.94	2.00	2.02
Chr1 3X	2.94	1.98	2.08	2.00	1.98	1.98	1.96	2.00
Chr2 3X	1.96	2.58	2.04	2.00	1.96	2.00	2.06	1.98
Chr3 3X	1.96	1.96	2.94	2.00	1.96	2.04	2.10	1.94
Chr4 3X	1.94	1.94	1.96	2.58	1.86	2.00	2.00	2.02
Chr5 3X	1.98	1.98	2.02	2.00	2.94	2.00	2.08	1.98
Chr6 3X	1.98	1.98	2.02	2.00	2.00	2.88	2.04	2.00
Chr7 3X	1.96	1.98	2.08	1.94	1.92	2.00	2.94	2.00
ChrR 3X	2.00	1.98	2.12	2.00	1.96	2.00	2.12	2.90
Chr1,6 3X	2.60	1.82	2.00	1.92	1.88	3.34	2.04	1.90
Chr3,6 3X	1.94	1.94	3.00	1.98	2.00	2.92	2.20	1.94
Chr4,5 3X	1.90	1.92	2.00	2.76	2.88	1.98	2.02	1.88
Chr4,7 3X	1.90	1.90	1.98	2.74	2.00	1.98	2.88	2.08
Chr5,7 3X	1.86	1.88	2.06	1.94	2.66	2.00	3.02	1.86
Chr6,7 3X	1.88	1.90	2.04	1.96	2.00	2.88	3.00	1.90
Chr5,6,7 3X	1.92	1.92	2.00	1.94	2.66	2.94	3.04	1.92
Chr1,4,5,7 3X	3.00	2.07	2.25	3.12	3.15	2.16	3.39	2.04
Chr1,2,3,5,R 3X	3.06	3.03	3.12	2.10	3.00	2.13	2.22	3.00
Chr6,R 4X	2.85	2.85	3.00	2.85	2.79	3.69	3.09	3.75

Chromosome copy number

1 2 3

c ddPCR

	Chromosome 1	2	3	4	5	6	7	R
euploid A	2.05	2.03	2.04	1.99	1.93	2.07	2.01	1.94
euploid B	2.00	2.06	2.01	2.00	2.00	2.04	1.94	1.98
euploid C	2.02	2.21	1.96	2.03	1.99	2.20	1.80	2.19
euploid D	2.10	2.21	1.98	1.68	1.76	2.06	2.08	1.82
euploid E	1.89	2.12	1.91	2.06	1.93	2.09	2.10	1.98
Chr3 1X	1.99	2.09	1.08	2.27	1.86	1.97	2.02	2.02
Chr1 3X	3.08	2.02	1.97	1.95	1.74	1.89	1.77	2.13
Chr2 3X	2.11	2.63	1.91	2.14	1.93	1.88	1.89	1.95
Chr3 3X	2.23	2.02	2.82	2.02	1.81	1.93	1.89	2.03
Chr4 3X	2.12	2.24	2.01	3.21	1.78	1.76	1.88	2.28
Chr5 3X	2.10	2.11	1.64	1.63	2.92	1.92	1.89	1.80
Chr6 3X	2.04	2.16	1.98	1.77	1.82	3.09	1.88	1.66
Chr7 3X	2.11	2.00	2.02	1.82	1.78	2.16	3.04	1.89
ChrR 3X	2.05	2.12	1.91	1.98	1.93	1.93	1.97	2.97
Chr1,6 3X	3.07	2.07	1.89	1.86	1.76	3.43	1.92	2.09
Chr3,6 3X	1.85	2.01	2.85	1.93	1.91	2.91	2.00	2.02
Chr4,5 3X	1.96	2.02	1.79	2.97	2.51	1.92	1.80	2.01
Chr4,7 3X	1.95	1.91	1.86	2.48	1.85	1.88	2.74	2.14
Chr5,7 3X	1.88	2.09	1.66	1.95	2.23	1.89	2.48	2.04
Chr6,7 3X	2.02	1.96	1.84	2.01	1.82	2.70	2.75	1.72
Chr5,6,7 3X	2.00	1.98	1.72	1.87	2.44	2.59	2.60	2.03
Chr1,4,5,7 3X	3.22	2.30	2.04	2.97	2.87	1.95	2.87	2.15
Chr1,2,3,5,R 3X	2.88	3.29	2.80	2.18	2.60	2.31	1.96	2.06
Chr6,R 4X	2.96	2.93	2.84	2.99	2.83	3.76	2.77	4.02

Chromosome copy number

1 2 3

Supplementary Figure 1

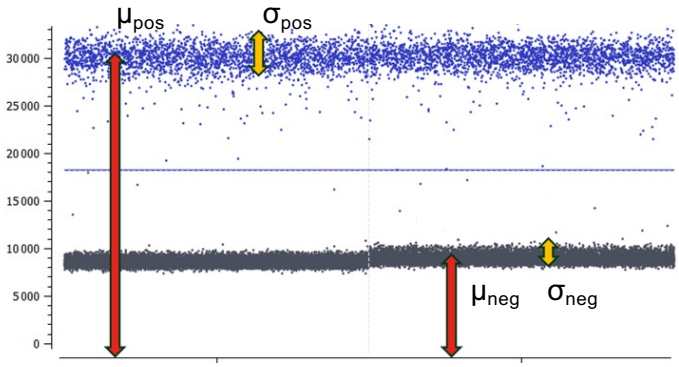

Separability score:

$$S = \frac{\mu_{pos} + \mu_{neg}}{\sqrt{\frac{p}{p-1}} * \sigma_{pos} + \sqrt{\frac{q}{q-1}} * \sigma_{neg}}$$

μ_{pos} = mean of the positive signals
μ_{neg} = mean of the negative signals
σ_{pos} = standard deviation of the positive signals
σ_{neg} = standard deviation of the negative signals
p = number of positive signals
q = number of negative signals

Supplementary Figure 2

a

	euploid A		Chr1,4,5,7 3X	
	simplex	multiplex	simplex	multiplex
Chr1	2.35	3.05	0.99	1.16
Chr2	1.31	1.14	0.87	1.15
Chr3	0.79	0.92	0.79	0.97
Chr4	0.44	0.35	0.69	0.57
Chr5	1.25	1.26	1.10	1.10
Chr6	0.56	0.41	0.00	0.00
Chr7	0.88	1.04	0.96	0.97
ChrR	1.01	0.64	0.93	0.48

Chromosome arm R:L ratio

0 1 2 3

b

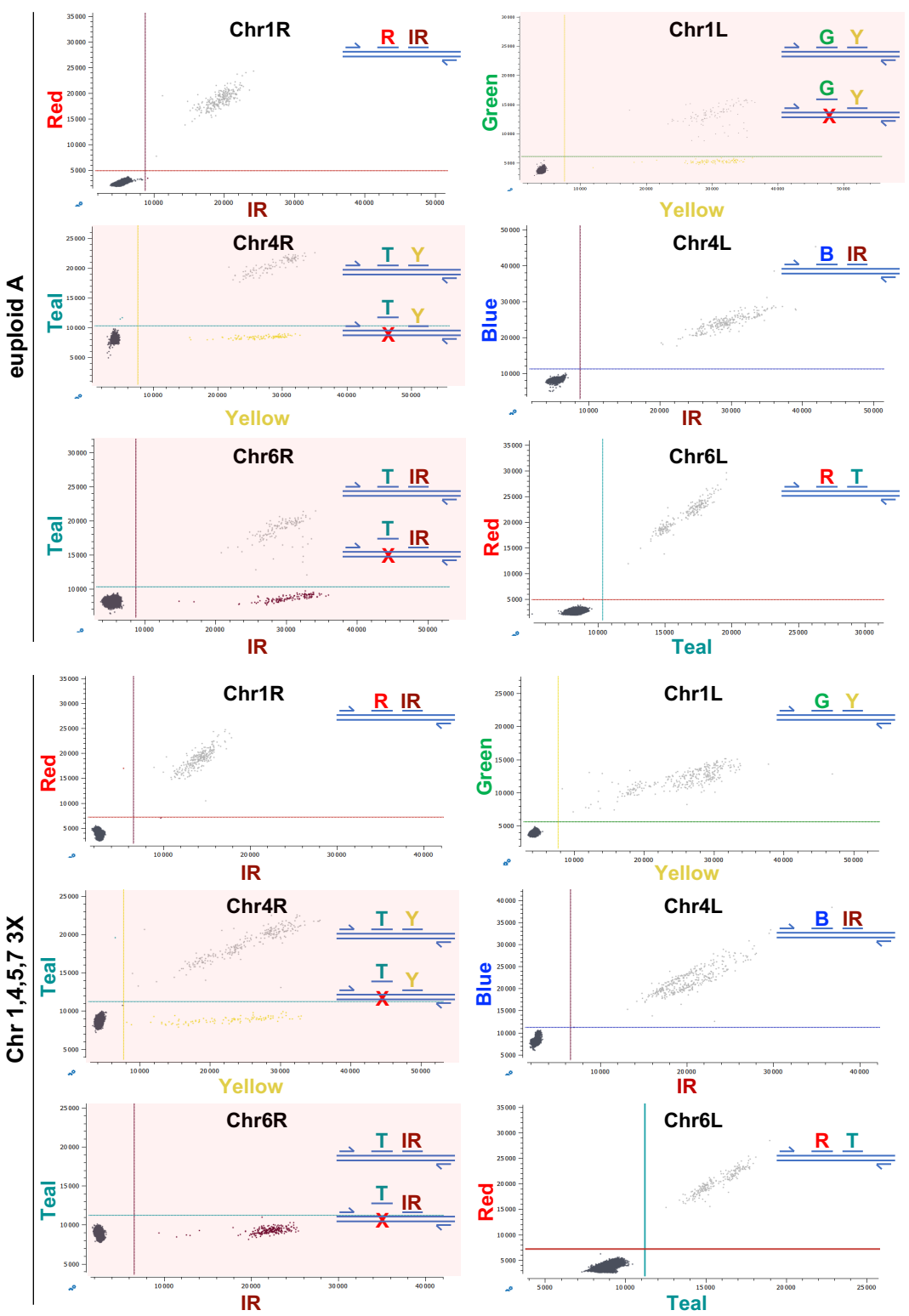

Supplementary Figure 3

a

		Chromosome arm															
		1L	1R	2L	2R	3L	3R	4L	4R	5L	5R	6L	6R	7L	7R	RL	RR
10 min	euploid A	6.50	6.10	8.70	5.80	6.90	7.20	5.60	4.90	5.50	6.10	6.10	4.70	3.30	6.40	5.10	6.90
	ChrR 3X	6.20	5.40	8.80	6.90	8.10	7.50	5.90	5.30	4.70	6.40	5.90	4.50	3.30	6.30	5.30	7.30
	Chr1,6 3X	5.80	6.30	8.40	5.40	7.20	7.40	5.50	5.30	5.40	5.30	5.90	4.90	3.30	6.80	4.60	6.90
	Chr1,4,5,7 3X	5.30	5.70	9.30	6.20	8.00	8.10	5.80	5.10	5.50	5.50	5.90	4.60	3.20	5.70	4.90	6.90
	Chr6,R 4X	6.10	5.30	9.80	7.20	8.40	8.20	5.30	5.80	4.50	7.00	7.40	4.20	3.20	5.70	5.70	7.80
15 min	euploid A	9.30	5.60	11.40	10.00	9.30	9.90	6.40	8.00	6.40	11.10	7.60	5.00	3.10	8.40	7.40	8.60
	ChrR 3X	7.80	5.30	10.80	9.20	9.90	9.10	6.40	6.50	5.30	8.90	7.40	4.40	3.20	6.70	6.60	7.90
	Chr1,6 3X	7.70	5.50	9.30	7.00	8.80	8.10	5.60	5.90	5.60	6.70	7.20	4.90	3.20	7.40	5.20	6.80
	Chr1,4,5,7 3X	9.40	5.60	11.50	10.60	9.30	10.90	6.90	7.60	6.40	10.90	8.00	5.40	3.30	8.20	7.40	7.90
	Chr6,R 4X	8.40	4.70	11.00	9.20	9.70	9.00	5.70	8.00	5.30	9.40	7.70	4.30	3.20	6.60	6.80	7.70

Separability score: 4 – 8 – 12

b

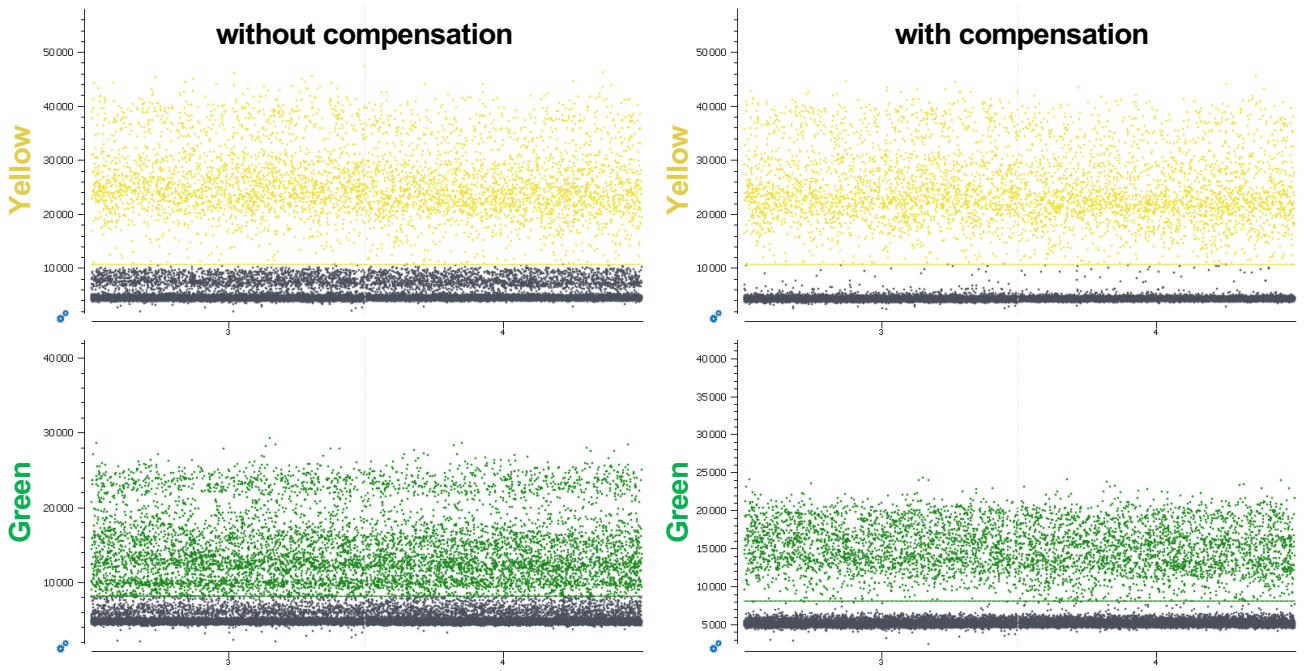

c

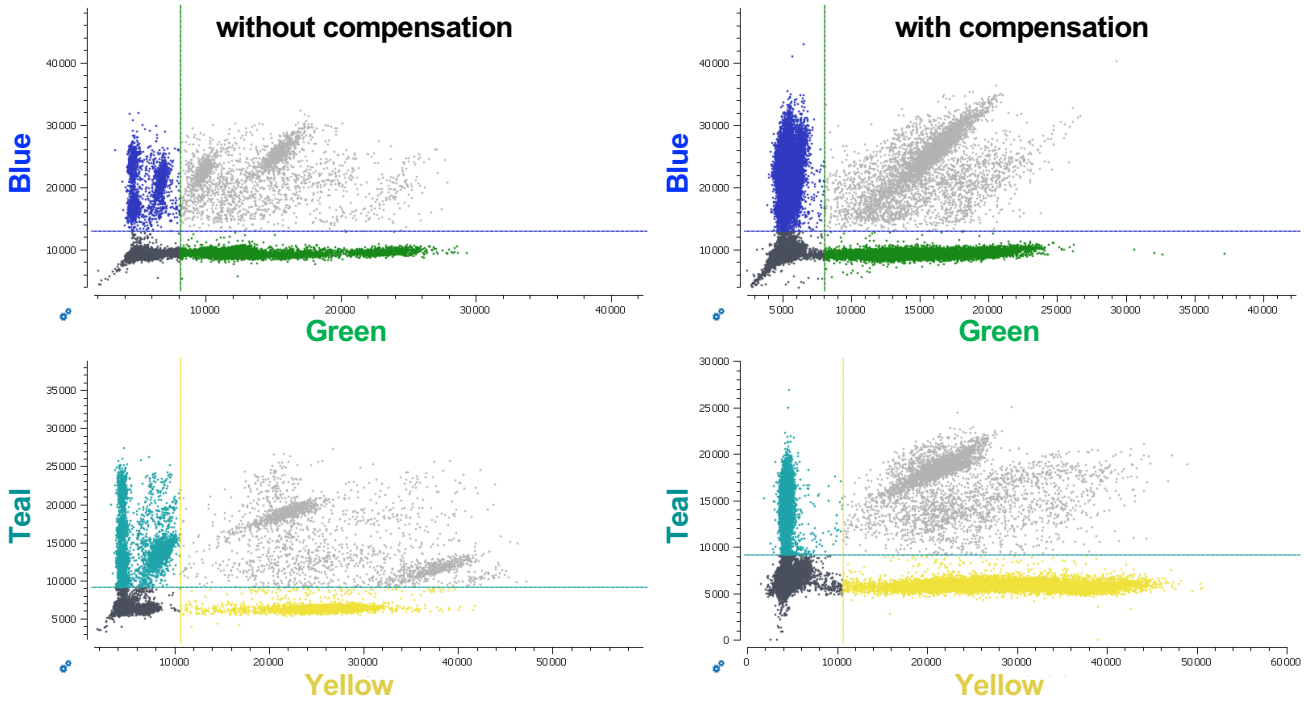

Supplementary Figure 4

a

Chromosome arm

		1L	1R	2L	2R	3L	3R	4L	4R	5L	5R	6L	6R	7L	7R	RL	RR
phenol chloroform 10 pg	euploid A	1.01	0.47	0.10	0.69	0.51	0.87	0.20	1.13	0.27	0.01	0.90	1.53	0.26	0.12	3.48	0.35
	Chr3 1X	0.47	0.07	1.50	0.16	1.10	1.81	0.16	0.56	1.90	2.51	0.56	0.95	1.41	1.10	1.59	1.88
	ChrR 3X	0.11	0.08	0.23	0.14	0.13	0.09	0.06	0.23	0.42	0.17	0.21	0.30	0.70	0.31	0.40	0.83
	Chr3,6 3X	0.03	0.36	1.16	0.53	1.27	0.35	0.70	1.41	0.17	0.12	0.79	0.61	0.70	0.34	2.26	1.09
	Chr6,R 4X	1.21	0.90	0.08	0.28	0.16	0.45	1.46	0.08	0.69	0.84	0.68	1.17	0.70	0.17	1.21	0.86
Qiagen 10 pg	euploid A	0.10	0.10	0.12	0.10	0.14	0.03	0.04	0.19	0.24	0.17	0.07	0.17	0.19	0.25	0.09	0.34
	Chr3 1X	0.39	0.20	0.13	0.32	0.52	0.14	0.20	0.36	1.15	0.21	0.18	0.87	0.23	0.26	0.11	0.58
	ChrR 3X	0.29	0.21	0.02	0.12	0.16	0.19	0.11	0.41	0.39	0.12	0.08	0.13	0.15	0.08	0.08	0.12
	Chr3,6 3X	0.09	0.07	0.08	0.05	0.21	0.08	0.32	0.09	0.06	0.13	0.12	0.12	0.04	0.03	0.16	0.16
	Chr6,R 4X	0.18	1.61	1.82	0.05	0.11	0.78	0.24	0.27	1.41	1.31	2.12	2.82	0.78	1.05	2.14	1.18
Qiagen 30 pg	euploid A	0.10	0.17	0.07	0.07	0.01	0.16	0.19	0.10	0.05	0.16	0.16	0.11	0.04	0.07	0.25	0.10
	Chr3 1X	0.13	0.17	0.15	0.06	0.19	0.13	0.06	0.18	0.19	0.24	0.09	0.12	0.10	0.16	0.24	0.08
	ChrR 3X	0.12	0.11	0.02	0.13	0.13	0.10	0.05	0.16	0.09	0.13	0.16	0.26	0.06	0.06	0.33	0.09
	Chr3,6 3X	0.18	0.37	0.11	0.02	0.18	0.31	0.02	0.04	0.13	0.09	0.22	0.24	0.24	0.12	0.50	0.05
	Chr6,R 4X	0.08	0.50	0.21	0.14	0.17	0.08	0.12	0.28	0.27	0.33	0.27	0.31	0.10	0.30	0.54	0.03

CNV standard deviation

0 1 2

b

Chromosome arm

		1L	1R	2L	2R	3L	3R	4L	4R	5L	5R	6L	6R	7L	7R	RL	RR
phenol chloroform 10 pg	euploid A	0.10	0.08	0.12	0.11	0.14	0.09	0.14	0.10	0.11	0.11	0.14	0.13	0.08	0.05	0.09	0.09
	Chr3 1X	0.07	0.15	0.06	0.12	0.04	0.04	0.12	0.13	0.09	0.18	0.09	0.08	0.18	0.16	0.10	0.14
	ChrR 3X	0.46	0.55	0.64	0.55	0.48	0.44	0.61	0.57	0.92	0.56	0.59	0.55	0.41	0.23	0.66	0.85
	Chr3,6 3X	0.12	0.07	0.15	0.09	0.23	0.14	0.18	0.12	0.11	0.11	0.11	0.22	0.15	0.01	0.09	0.14
	Chr6,R 4X	0.02	0.10	0.09	0.13	0.04	0.05	0.07	0.13	0.10	0.16	0.12	0.20	0.12	0.04	0.20	0.16
Qiagen 10 pg	euploid A	1.05	1.20	1.22	1.27	1.22	1.25	1.23	1.17	1.11	1.19	1.29	1.37	1.21	1.29	1.20	1.25
	Chr3 1X	0.94	0.91	0.99	0.93	0.49	0.56	1.05	0.91	0.67	0.85	0.64	0.96	0.83	0.84	1.03	0.87
	ChrR 3X	1.08	1.11	1.04	1.16	1.04	1.05	1.04	1.07	1.02	1.19	0.99	1.10	1.17	1.13	1.66	1.57
	Chr3,6 3X	1.33	1.53	1.45	1.57	2.33	2.30	1.48	1.37	1.43	1.45	2.10	2.32	1.54	1.57	1.51	1.40
	Chr6,R 4X	1.64	1.89	1.60	1.71	1.75	1.68	1.72	1.47	1.61	1.41	1.49	2.25	1.45	1.57	2.46	2.21
Qiagen 30 pg	euploid A	2.17	2.21	2.34	2.32	2.17	2.17	2.36	2.24	2.29	2.30	2.31	2.47	2.31	2.43	2.44	2.25
	Chr3 1X	1.98	2.47	2.15	2.20	1.08	1.07	2.49	2.57	1.90	1.43	0.99	2.37	1.84	1.95	2.47	2.01
	ChrR 3X	2.12	2.86	2.19	2.46	1.98	2.25	2.37	2.03	2.28	2.01	1.94	2.66	2.11	2.04	4.01	2.98
	Chr3,6 3X	2.16	2.91	2.22	2.40	3.38	3.50	2.23	2.23	2.34	2.15	3.00	4.08	2.04	2.21	2.97	2.27
	Chr6,R 4X	2.45	3.75	2.65	2.87	2.32	2.60	2.84	2.79	2.73	2.05	1.94	4.14	2.18	2.13	4.76	3.18

Fraction of positive droplets (%)

0 1 2 3

c

Chromosome arm

		1L	1R	2L	2R	3L	3R	4L	4R	5L	5R	6L	6R	7L	7R	RL	RR
phenol chloroform 10 pg	euploid A	1.40	1.98	2.40	1.87	2.35	1.27	2.85	2.80	2.19	2.01	1.96	1.74	1.82	1.26	3.87	2.13
	Chr3 1X	1.67	3.06	1.95	2.11	1.23	1.73	2.11	2.62	2.68	1.77	1.38	0.67	3.00	2.77	2.90	1.33
	ChrR 3X	1.89	1.93	2.51	1.81	1.73	1.73	2.12	2.07	2.94	2.05	2.34	2.20	1.71	1.16	2.44	2.78
	Chr3,6 3X	1.98	0.94	3.22	1.02	2.90	2.44	2.50	3.00	1.92	1.88	1.24	3.16	2.89	0.44	3.00	1.42
	Chr6,R 4X	0.86	2.22	1.66	2.20	0.68	1.11	1.82	2.34	2.07	2.59	1.91	4.01	1.92	0.69	3.14	2.60
Qiagen 10 pg	euploid A	1.88	2.01	1.93	2.14	2.07	2.06	2.00	1.86	1.91	2.06	2.15	2.11	2.10	1.96	1.93	1.88
	Chr3 1X	2.26	1.85	2.15	2.28	1.34	1.30	2.22	1.80	2.13	2.02	1.80	2.61	2.20	1.69	2.28	2.26
	ChrR 3X	1.86	2.00	1.87	2.16	1.94	1.83	1.79	1.74	2.04	2.26	1.83	1.87	2.22	2.00	3.03	2.91
	Chr3,6 3X	1.78	1.92	1.97	2.13	3.07	3.02	1.99	1.80	1.84	1.87	2.87	3.04	2.02	2.04	1.93	1.77
	Chr6,R 4X	2.93	3.95	3.72	2.98	3.13	2.34	2.98	2.74	1.84	2.08	2.40	5.37	3.60	2.05	5.26	3.07
Qiagen 30 pg	euploid A	1.95	2.21	2.00	2.00	1.89	1.94	2.02	1.96	1.88	1.90	2.05	2.03	1.98	2.06	2.27	1.93
	Chr3 1X	1.97	2.06	2.01	2.10	1.13	0.99	2.38	2.36	1.73	2.01	1.83	2.12	2.24	1.90	2.12	1.94
	ChrR 3X	1.93	2.32	2.00	2.33	1.90	1.96	2.05	1.96	1.84	1.94	1.91	2.09	1.99	1.80	3.36	2.72
	Chr3,6 3X	1.83	2.00	1.93	2.13	2.91	2.75	1.94	1.97	1.84	1.97	2.81	3.05	1.95	1.92	2.27	1.96
	Chr6,R 4X	2.88	3.26	2.80	3.26	2.82	2.80	3.10	3.08	2.74	2.91	3.48	4.05	2.93	2.45	4.78	3.55

Chromosome copy number

1 2 3

Supplementary Figure 5

a

Chromosome arm

	1L	1R	2L	2R	3L	3R	4L	4R	5L	5R	6L	6R	7L	7R	RL	RR
none	0.23	0.25	0.07	0.24	0.18	0.04	0.21	0.63	0.09	0.21	0.40	0.07	0.10	0.09	0.24	0.17
EcoRI	0.05	0.07	0.32	0.34	0.24	0.09	0.04	0.17	0.16	0.16	0.27	0.12	0.06	0.02	0.20	0.19
BamHI	0.12	0.23	0.09	0.09	0.24	0.07	0.32	0.11	0.13	0.35	0.16	0.28	0.11	0.10	0.15	0.21
HindIII	0.33	0.31	0.27	0.22	0.10	0.23	0.23	0.13	0.28	0.20	0.30	0.16	0.14	0.35	0.04	0.11
PstI	0.17	0.02	0.18	0.19	0.26	0.14	0.14	0.07	0.07	0.10	0.17	0.09	0.25	0.06	0.20	0.07
PstI+BamHI	0.07	0.24	0.10	0.11	0.28	0.07	0.08	0.27	0.15	0.29	0.15	0.14	0.16	0.33	0.16	0.26
PstI+EcoRI	0.14	0.03	0.18	0.06	0.15	0.01	0.20	0.16	0.15	0.07	0.07	0.11	0.08	0.18	0.19	0.17
PstI+HindIII	0.10	0.10	0.12	0.10	0.14	0.03	0.04	0.19	0.24	0.17	0.07	0.17	0.19	0.25	0.09	0.34
BamHI+EcoRI	0.18	0.10	0.11	0.12	0.23	0.07	0.12	0.10	0.18	0.11	0.07	0.19	0.20	0.11	0.09	0.18
BamHI+HindIII	0.14	0.11	0.42	0.42	0.03	0.12	0.15	0.08	0.07	0.16	0.13	0.07	0.28	0.11	0.36	0.19
HindIII+EcoRI	0.04	0.19	0.05	0.11	0.28	0.25	0.18	0.25	0.29	0.10	0.16	0.15	0.22	0.14	0.33	0.11

CNV standard deviation

0 1 2

b

Chromosome arm

	1L	1R	2L	2R	3L	3R	4L	4R	5L	5R	6L	6R	7L	7R	RL	RR
none	5.82	6.25	8.86	7.99	8.47	8.01	7.22	5.45	5.84	9.70	6.17	6.22	3.14	8.13	5.50	6.47
EcoRI	5.93	6.30	9.42	7.40	8.72	7.93	6.69	6.05	5.46	9.33	6.29	5.92	3.10	7.85	5.42	6.65
BamHI	7.16	8.69	10.89	8.49	9.96	8.78	8.06	6.79	6.98	10.24	7.93	6.97	3.35	8.04	6.80	7.26
HindIII	6.45	7.59	10.02	6.48	9.40	7.30	7.33	5.80	5.50	7.76	6.89	6.12	3.35	7.80	5.17	6.07
PstI	7.57	9.13	9.86	8.01	9.82	7.87	8.35	6.67	6.04	9.63	8.61	6.82	3.25	8.36	6.44	7.11
PstI+BamHI	6.58	7.95	10.85	7.59	9.70	7.82	7.71	6.80	5.83	9.91	6.93	6.22	3.26	8.38	5.86	7.39
PstI+EcoRI	6.84	7.71	9.50	8.88	9.50	8.49	7.56	6.12	6.14	10.96	7.53	6.14	3.26	9.06	6.46	7.90
PstI+HindIII	8.12	8.22	11.36	10.13	11.15	10.53	9.15	7.17	7.17	12.98	8.23	7.21	3.32	10.61	6.46	8.34
BamHI+EcoRI	5.28	6.81	9.37	7.02	8.53	7.34	6.88	5.29	5.19	8.41	6.37	5.95	3.44	7.47	4.81	6.12
BamHI+HindIII	5.95	7.52	8.77	6.10	8.06	8.00	6.68	5.28	5.49	7.08	6.34	5.89	3.17	7.17	4.31	6.32
HindIII+EcoRI	6.21	7.25	9.53	7.28	9.79	7.99	7.52	5.57	5.34	9.31	6.78	6.29	3.16	7.94	5.49	6.48

Separability score

4 8 12

c

Chromosome arm

	1L	1R	2L	2R	3L	3R	4L	4R	5L	5R	6L	6R	7L	7R	RL	RR
none	1.08	1.16	0.93	0.97	0.89	0.87	1.10	1.00	0.78	0.78	0.80	0.81	0.89	0.91	0.90	0.75
EcoRI	1.22	1.37	1.28	1.32	1.30	1.26	1.37	1.25	1.26	1.34	1.30	1.29	1.33	1.28	1.36	1.17
BamHI	0.83	0.84	0.69	0.76	0.87	0.84	0.98	0.86	0.88	0.87	0.83	0.86	0.94	0.85	0.87	0.85
HindIII	0.89	1.08	1.01	1.14	1.11	1.00	1.14	1.05	0.89	0.99	1.03	0.98	0.99	1.01	1.16	0.91
PstI	0.94	1.28	1.23	1.30	1.18	1.19	1.25	1.13	1.17	1.27	1.21	1.26	1.45	1.31	1.40	1.19
PstI+BamHI	0.87	0.92	0.97	0.99	0.93	0.90	1.02	0.96	0.91	0.89	0.88	0.99	0.91	0.97	1.02	0.91
PstI+EcoRI	1.22	1.30	1.27	1.14	1.19	1.17	1.24	1.16	1.19	1.26	1.35	1.25	1.27	1.21	1.26	1.10
PstI+HindIII	0.81	0.86	0.85	0.91	0.89	0.89	0.86	0.81	0.82	0.88	0.93	0.94	0.89	0.90	0.85	0.87
BamHI+EcoRI	1.14	1.12	1.20	1.24	1.14	1.16	1.31	1.12	1.14	1.15	1.19	1.27	1.19	1.23	1.17	1.17
BamHI+HindIII	1.02	1.20	1.25	1.23	1.18	1.12	1.21	1.15	1.12	1.20	1.17	1.21	1.16	1.14	1.31	1.00
HindIII+EcoRI	1.17	1.23	1.20	1.20	1.18	1.16	1.32	1.16	1.27	1.24	1.21	1.27	1.22	1.19	1.36	1.10

Fraction of positive droplets (%)

0 1 2 3

d

Chromosome arm

	1L	1R	2L	2R	3L	3R	4L	4R	5L	5R	6L	6R	7L	7R	RL	RR
none	2.39	2.55	2.07	2.21	2.03	1.95	2.43	2.09	1.76	1.80	1.90	1.83	1.97	2.00	2.03	1.72
EcoRI	1.91	2.11	2.17	2.15	2.09	1.97	2.11	1.92	1.96	2.13	1.97	1.97	2.06	1.98	2.09	1.75
BamHI	2.05	1.90	1.69	1.75	2.11	1.93	2.41	2.01	2.03	2.16	1.89	2.00	2.23	1.95	2.09	2.04
HindIII	1.62	2.09	2.19	2.25	2.15	1.92	2.30	2.05	1.66	2.00	1.94	1.86	1.91	1.95	2.25	1.73
PstI	1.92	2.04	2.16	2.13	2.04	1.82	2.06	1.78	1.92	2.10	1.86	2.00	2.45	2.07	2.22	1.91
PstI+BamHI	1.82	1.83	2.13	2.12	2.09	1.92	2.18	1.97	1.92	1.95	1.82	2.05	2.01	2.16	2.10	1.86
PstI+EcoRI	2.05	2.13	2.02	1.87	1.92	1.94	2.12	1.96	1.95	2.08	2.24	2.06	2.08	1.95	2.03	1.86
PstI+HindIII	1.88	2.01	2.13	2.14	2.07	2.06	2.00	1.86	1.91	2.06	2.15	2.11	2.10	1.96	1.93	1.88
BamHI+EcoRI	1.91	1.88	2.11	2.13	2.03	1.96	2.27	1.90	1.88	2.00	2.03	2.13	2.08	2.08	1.97	1.96
BamHI+HindIII	1.79	2.05	2.35	2.30	2.03	1.93	2.05	2.00	1.91	2.02	2.02	2.06	2.11	2.00	2.12	1.80
HindIII+EcoRI	1.95	2.03	1.94	2.01	2.05	1.84	2.21	1.92	2.21	2.09	2.07	2.06	2.11	1.94	2.17	1.80

Chromosome copy number

1 2 3